Marwa Rebei, Olga Kočková, Matouš Řehák, Sabina Abbrent, Anna Vykydalová, Jan Honzíček, Petra Ecorchard, Hynek Beneš (2024). Accelerating effect of metal ionic liquids for epoxy-anhydride copolymerization. *European Polymer Journal*. Volume 212, 27 May 2024, 113077. DOI: 10.1016/j.eurpolymj.2024.113077

Accelerating effect of metal ionic liquids for epoxy-anhydride copolymerization

Marwa Rebei[†], *Olga Kočková*[†], *Matouš Řehák*[§], *Sabina Abbrent*[†], *Anna Vykydalová*[ϕ], *Jan Honzíček*[Δ], *Petra Ecorchard*[ϕ], *Hynek Beneš*[†,*]

[†]Institute of Macromolecular Chemistry, Czech Academy of Sciences, Heyrovského nám. 2, Prague 6, 162 06, Czech Republic

[ϕ]Institute of Inorganic Chemistry, Czech Academy of Sciences, Husinec-Řež 1001, 250 68 Řež, Czech Republic

[§] Department of General and Inorganic Chemistry, Faculty of Chemical Technology, University of Pardubice, Studentská 573, 532 10, Pardubice, Czech Republic

[Δ]Institute of Chemistry and Technology of Macromolecular Materials, Faculty of Chemical Technology, University of Pardubice, Studentská 573, 532 10, Pardubice, Czech Republic

KEYWORDS: ionic liquid, epoxy copolymerization, anhydride, epoxy cross-linking, epoxy kinetics

ABSTRACT

In this study, we synthesized 1-butyl-3-methylimidazolium metal-based ionic liquids (MILs) incorporating $(FeCl_4)^-$, $(ZnCl_4)^{2-}$, and $(CoCl_4)^{2-}$ as anions. The resulting MILs were employed as accelerators in the reaction between bisphenol diglycidyl ether (DGEBA) and methylhexahydrophthalic anhydride (MHHPA), exhibiting higher reactivity. A comprehensive comparison with conventional catalysts, such as 1-methylimidazole (1MIM) and 1-butyl-3-methylimidazolium chloride (BMIMCl), was studied using dynamic differential scanning

calorimetry (DSC) and near-infrared spectroscopy (NIR). The formulations of DGEBA/MHHPA/MILs revealed a faster overall polymerization reaction at low temperatures (60 to 80 °C). To unravel the initiation mechanism of the epoxy curing, MALDI-TOF was employed in a model reaction using phenylglycidyl ether (PGE) as a monofunctional epoxy, revealing a distinct initiation mechanism for MILs compared to 1MIM and BMIMCl. Additionally, the molar content of MILs in the DGBEA-MHHPA reaction was studied via dynamic DSC, showcasing an increase in the onset temperature (T_{onset}) as the mol% decreases. Kinetics studies were also investigated using isothermal DSC, based on the Kamal–Sourour model, and yielded kinetic parameters (e.g. activation energy, E_a). Furthermore, the thermomechanical properties of the final epoxy networks (i.e., glass transition temperature, T_α, cross-link density, v_e, and char yield) were examined. Our comprehensive exploration establishes MILs as effective catalysts in epoxy curing, exerting influence on the reaction mechanism, kinetics, and final thermomechanical properties.

Introduction

The alternating copolymerization of epoxides and cyclic anhydrides has always been a promising and bourgeoning area of research [1] due to its capability of providing thermosetting materials exhibiting excellent thermal, mechanical and optical properties, which allow the production of high-tech engineering materials for electrical and electronic applications and composite matrices for aerospace and transport.[2–5] Unlike other curing agents, anhydride hardeners can provide highly cross-linked epoxy networks exhibiting a high glass transition temperature (T_g), low reaction heat release and reduced shrinkage [2,6]. Nevertheless, the epoxy-anhydride systems suffer from the limitation of being less reactive, requiring high curing temperatures, long curing cycles and associated high energy costs. It is therefore necessary to use suitable accelerators / catalysts to accelerate the polymerization.

The most common accelerators of the epoxy-anhydride reaction are tertiary amines [7,8] or imidazoles [9]. Especially 1-substituted and 1-unsubstituted imidazoles are promising initiators of the anionic alternating copolymerization of epoxides with cyclic anhydrides.[10,11] Short pot life, too high curing temperatures and low stability are the main drawbacks of imidazoles. Therefore, solutions are sought to improve their processability by stabilizing the lone pair of nitrogen atoms. One strategy involves the preparation of metal-imidazole complexes. In particular, zinc and cobalt metals have proved to be efficient anionic initiators for the ring-opening of epoxides, specifically complexes of Zn/imidazole type [M(imidazole)$_2$(anion)$_2$].[12] Unfortunately, metal-imidazole complexes are mostly crystalline substances with very low solubility in epoxy systems.[13] Thus, the use of a solvent is often required, which limits applicability due to the release of volatile compounds.[14,15] The use of discrete metal and rare earth metal complexes enable well-controlled polymerization progress [1], but cost and toxicity often limit their widespread use.[16]

To overcome the above-mentioned drawbacks, ionic liquids (ILs) have become interesting in terms of their use as catalysts to provide a ‘’greener’’ and solvent-free one-pot reaction medium.[17] They are efficient catalysts/initiators for ring-opening polymerization.[18–20] Their structure combines a cation (imidazolium, pyridinium, phosphonium, etc.) associated with a variety of anions (halogens, phosphates, imide, triflate).[21,22] Different combinations of cations and anions give rise to physical property tuning, resulting in outstanding properties such as excellent chemical and thermal stability, negligible vapor pressure, and good conductivity.[23,24] As a result, ILs are now considered as new accelerators for the epoxy cross-linking in a solvent-free medium.[17,25,26]

Recently, a new class of ILs, metal-based ionic liquids (MILs), has been explored containing a metal atom in IL-anionic part.[27] The introduction of a metal into the imidazolium-based IL increases its Lewis acid character.[28–30] Till now, only a few applications of MILs as catalysts / accelerators have been reported in the literature; e.g. the use of Ln-containing ILs in electric and magnetic switchable devices [27], the application of aluminum, palladium, zinc, and iron-based ILs for polystyrene formation [31,32], or the degradation of PET via cobalt-based IL.[33] Typical MILs is composed of $[MX_4]^{2-}$ anions, where M can be various metals, e.g. Zn, Co, Fe, Ni, and Cu, and X is a halide, usually chloride, tetrahedrally coordinating a metal atom.[27] Bis(1-alkyl-3-methylimidazolium)tetrahalogenomanganate $[C_{2\text{-}4}mim]_2[MnCl_4]$ [34], ethylmethylimidazolium iron(III)chloride [EMIMCl]$FeCl_3$ [30], and $[BMIM]_2[CoCl_4]$ and $[BMIM]_2[ZnCl_4]$ are typical examples of synthesized MILs.[33] In addition, it has been shown that the acid-base character of MILs can affect their catalytic activity.[27] A recent study based on the epoxy-anhydride reaction catalyzed by magnetic ILs, phosphonium- and imidazolium-based ILs with $FeCl_4$ anions, suggested a significant catalytic effect of these ILs toward epoxy–anhydride curing.[35]

Based on our previous study showing a catalytic ability of the chloride anion of imidazolium ILs[36], in this work, we hypothesize an accelerating effect of imidazolium MILs for the epoxy–anhydride copolymerization due to the enhanced Lewis acidity character of MIL-anions bearing Fe, Zn and Co atoms. Therefore, a series of MILs was synthesized and used as accelerators for epoxy – anhydride cross-linking under solvent-free conditions. A detailed kinetic investigation using differential scanning calorimetry (DSC) and near-infrared (NIR) spectroscopy was performed and kinetic parameters were determined via isothermal modeling. MALDI TOF mass spectrometry enabled us to propose a mechanism of MILs-induced epoxy – anhydride copolymerization. Finally, the produced epoxy networks were characterized using dynamic mechanical analysis (DMA) and thermogravimetric analysis (TGA).

EXPERIMENTAL SECTION

Materials

Bisphenol A diglycidyl ether epoxy resin DGEBA (D.E.R 332) with an epoxy equivalent weight of 179 g/mol, was supplied by DOW chemicals. Hexahydro-4-methylphthalic anhydride (MHHPA, 96%) and 1-methylimidazole (1MIM, 99%) were provided by Sigma Aldrich. 1-butyl-3-methylimidazolium chloride (BMIMCl, 99%) was supplied by Iolitech. Iron(III) chloride (anhydrous, 98%) and cobalt(II) chloride (anhydrous, 99%) were supplied by Acros Organics, zinc(II) chloride (anhydrous, p.a.) was provided by Lach-Ner.

Synthesis of epoxy-anhydride networks

In the present study, metal-based ionic liquids (MILs) incorporating Zn(II), Co(II), and Fe(II) were synthesized in accordance with established methodologies outlined in prior reports.[37–41] The comprehensive details of the synthesis procedure and characterization methods

are described in the Supporting Information (SI). Subsequently, the epoxy monomer (DGEBA) and anhydride (MHHPA) were mixed, in an equimolar ratio, with various amounts (from 0.05 to 5.00 mol%) of 1-methylimidazole (1MIM), 1-butyl-3-methylimidazolium chloride (BMIMCl), 1-butyl-3-methylimidazolium tetrachloroferrate (BMIM)$FeCl_4$, 1-butyl-3-methylimidazolium tetrachlorocobaltate $(BMIM)_2CoCl_4$, or 1-butyl-3-methylimidazolium tetrachlorozincate $(BMIM)_2ZnCl_4$. The resultant mixture underwent homogenization for 10 min, followed by casting into open aluminum molds. The curing process at 80 °C for 4 h, 150 °C for 2 h, and finally, at 180 °C for 4 h in a vacuum oven to avoid bubbles formation and mitigate undesired oxidation. For comparative analysis of overall reactivity and final material properties, reference samples, DGEBA/MHHPA/1MIM using the conventional catalyst 1-methylimidazole [42] along with DGEBA/MHHPA/BMIMCl were employed. The structural representations and acronyms for the catalysts used are elucidated in Figure 1.

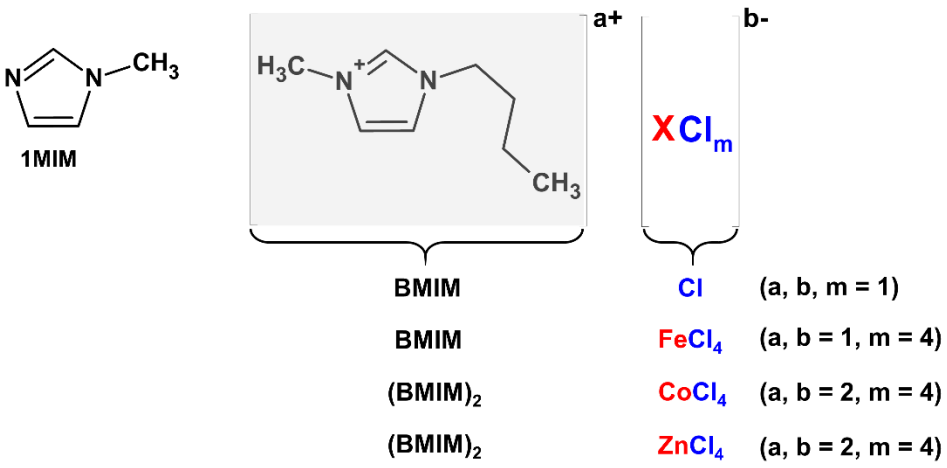

Figure 1. Structures and acronyms of the ionic liquids used.

Model reaction of monofunctional epoxy and anhydride

1,2-Epoxy-3-phenoxypropane (phenyl glycidyl ether, PGE, 99%, Sigma-Aldrich) and MHHPA were mixed in an equimolar ratio and then a 2.70 mol% of 1MIM, BMIMCl, (BMIM)$FeCl_4$, $(BMIM)_2CoCl_4$, or $(BMIM)_2ZnCl_4$ was added and homogenized using a

magnetic stirrer. The reaction was carried out at 80 °C. The reaction mixture was regularly sampled and the progress of the reaction was monitored using FTIR and MALDI-TOF mass spectrometry.

Monitoring of the epoxy-anhydride cross-linking

Near-IR spectra (NIR) were acquired using a Nicolet iS50 FTIR spectrometer (Thermo Fisher Scientific) in transmission mode using a HT-32 heating cell and homemade cuvettes made of two glass slides and tape as a spacer to determine the thickness of the sample (d = 1 mm). Dynamic runs were performed from 30 to 300 °C at a heating rate of 5 °C/min. The isothermal runs were carried out at 60 °C for 2 h. In both types of time-resolved experiments, the spectra were collected every 20 s (32 scans per spectrum, a data spacing of 1 cm^{-1}). The collected spectra were integrated using a fixed two-point baseline in the regions of 4502−4568, 4803−4867, 5100−5190, 5210−5272, and 6800−7132 cm^{-1} to monitor epoxy, anhydride, ester, moisture, and hydroxy groups, respectively. The integral intensities obtained were calibrated based on the intensity of the integrated reference band in the region of 4592−4652 cm^{-1}. The conversions of epoxy, anhydride, ester, moisture, and hydroxy groups are defined as follows (equations 1-5):

$$\alpha(t)_{Epoxy} = 1 - \frac{A_{4530}(t)}{A_{5430}(t=0)} \Big/ \frac{A_{4622}(t)}{A_{4622}(t=0)} \quad (1)$$

$$\alpha(t)_{Anhydride} = 1 - \frac{A_{4828}(t)}{A_{4828}(t=0)} \Big/ \frac{A_{4622}(t)}{A_{4622}(t=0)} \quad (2)$$

$$\alpha(t)_{Ester} = \frac{A_{5158}(t)}{A_{5158}(max)} \Big/ \frac{A_{4622}(t)}{A_{4622}(t=0)} \quad (3)$$

$$\alpha(t)_{Moisture} = 1 - \frac{A_{5252}(t)}{A_{5252}(t=0)} \Big/ \frac{A_{4622}(t)}{A_{4622}(t=0)} \quad (4)$$

$$\alpha(t)_{Hydroxy} = \frac{A_{6985;7030}(t)}{A_{6985;7030}(max)} \Big/ \frac{A_{4622}(t)}{A_{4622}(t=0)} \quad (5)$$

Dynamic and isothermal differential scanning calorimetry (DSC) measurements of the reactive mixtures were performed using a DSC calorimeter (Q 2000, TA Instruments) calibrated for indium. Samples (5-15 mg) were hermetically sealed in Tzero aluminum pans with a pinhole and measured under a nitrogen flow of 50 mL/min. Dynamic DSC runs were performed from 20 to 300 °C at a heating rate of 5 °C/min.

The conversion curves (Conversion vs time) were obtained by measuring the reactive mixture in DSC using dynamic and isothermal runs. Additional ramp DSC run of 10 °C /min was performed to measure the residual reaction heat (ΔH_{res}) after isothermal curing. The conversion of epoxy groups (α) was calculated from the DSC data according to equation (6) [43]:

$$\alpha(t)_{\text{DSC}} = \frac{\int_0^t \frac{dH}{dt} dt}{\Delta H_{total}} + \left(1 - \frac{\Delta H_{res} + \Delta H_{iso}}{\Delta H_{total}}\right) \quad (6)$$

where dH/dt is the instantaneous time derivative of the heat during the dynamic or isothermal run, ΔH_{total} is the total enthalpy of the reaction determined from the dynamic DSC runs and ΔH_{iso} is the heat of reaction measured from the isothermal DSC scans.

Then, the epoxy-anhydride cross-linking was modelled using Kamal-Sourour model[44] according to equation (7):

$$\frac{d\alpha}{dt} = (k_1 + k_2 \alpha^m)(1 - \alpha)^n \quad (7)$$

where k_1 and k_2 are rate constants for the non-catalytic and the autocatalytic reactions respectively, and m and n are partial reaction orders. A numerical integration using the 4th order Runge–Kutta method was used to calculate model predicted α_{sim} values for each tested temperature. These values were then compared to experimentally found α_{exp} (from isothermal DSC) using the ordinary least squares (OLS) error (Microsoft Excel)[45]:

$$OLS = \sum_i [\alpha_{exp} - \alpha_{sim}]_i^2 \quad (8)$$

This OLS criterion was then minimized using the GRG algorithm (Microsoft Excel). By this procedure, the reaction rates of non-catalysed (k_1) and auto-catalysed (k_2) reactions were determined for each temperature. Arrhenius equation was used for the determination of the activation energy of the reactions:

$$k = A \exp\left(\frac{E_a}{RT}\right) \quad (9)$$

where A is the pre-exponential factor, E_a is the activation energy, and R is the universal gas constant.

Characterizations

Fourier transmission infrared spectroscopy (FTIR) measurements of the obtained samples were performed using a Spectrum 100 spectrometer (PerkinElmer) equipped with a mercury−cadmium−telluride (MCT) detector and universal ATR (attenuated total reflectance) accessory with a diamond prism. The spectra were averaged over 32 scans with a selected resolution of 4 cm^{-1}. The disappearance of the peak at 915 cm^{-1} is followed during the reaction as it is attributed to the C-O stretching of the oxirane group.[46]

MALDI-TOF mass spectra were acquired with the UltrafleXtreme TOF – TOF mass spectrometer (Bruker Daltonics, Bremen, Germany) equipped with a 2000 Hz smartbeam-II laser (355 nm) using the positive ion reflectron mode. Panoramic pulsed ion extraction and external calibration were used for molecular weight assignment. The dried droplet method was used in which the solutions of the sample (10 mg mL^{-1}), matrix DHB (2,5-Dihydroxybenzoic acid; 20 mg mL^{-1}), and ionizing agent sodium trifluoroacetate (CF_3COONa; 10 mg mL^{-1}) in THF were mixed in the volume ratio 4:20:1. 1 μL of the mixture was deposited on the ground-steel target.

Dynamic-mechanical and thermal analysis (DMTA) of the cured epoxy samples was measured on an ARES G2 rheometer (TA Instruments). The temperature dependence of

complex shear modulus (G^*) was determined on rectangular samples (20x10x2 mm) using oscillatory shear deformation (0.01 – 0.1 % strain) at 1 Hz frequency from 25 °C to 220 °C at a temperature ramp rate of 3 °C/min. The main transition temperature (T_α) was determined as the tan δ peak maximum. The cross-link density (v_e) is calculated by equation (10):

$$v_e = G'/RT \quad (10)$$

where G' is the storage modulus of the networks in the rubbery plateau at $T = T_\alpha + 50$ °C, R is the universal gas constant, and T is the absolute temperature in Kelvin. The average molecular mass between cross-links (M_c) was calculated by equation (11):

$$M_c = \rho RT/G'_R \quad (11)$$

Where ρ is the calculated density, T is the absolute temperature in Kelvin at $T_\alpha + 50$ °C, and G'_R is the storage modulus of the networks in the rubbery plateau at T.

Thermogravimetric analysis (TGA) was carried out with a thermogravimetric analyser Pyris 1 TGA (PerkinElmer). A sample of ca. 5 mg was heated from 30 °C to 800 °C at a heating rate of 10 °C/min in nitrogen flow (25 cm^3/min).

RESULTS AND DISCUSSION

Non-isothermal epoxy-anhydride cross-linking

The synthesized metal-based ionic liquids (MILs) were applied as accelerating agents for the epoxy-anhydride (DGEBA/MHHPA) reaction and compared with a metal-free IL (BMIMCl) and a commercially used catalyst (1MIM).[42,43,47] First, the cross-linking of DGEBA/MHHPA reactive mixtures with 2.7 mol% of the accelerating agents was studied using

non-isothermal (dynamic) DSC at a heating rate of 5 °C/min. Figure 2a plots the DSC runs showing a significant exothermic peak related to the epoxy-anhydride reaction (except for the accelerator-free system showing only a small exotherm above 230 °C due to non-catalytic curing[48], which leads to partially cured epoxide with low final T_g, Table S2, entry 1). Both reference systems (DGEBA/MHHPA/1MIM and DGEBA/MHHPA/BMIMCl) showed similar one exothermic peak with a T_{onset} approximately at 100 °C (Table S2, entries 2 and 3). The MILs-containing systems showed a shift of the main exothermic peak toward lower (DGEBA/MHHPA/$BMIMFeCl_4$ and DGEBA/MHHPA/$(BMIM)_2CoCl_4$) or higher (DGEBA/MHHPA/$(BMIM)_2ZnCl_4$) temperature, while their determined ΔH_{total} values were slightly lowered compared to conventionally-catalyzed system (Figure 2a and Table S2).

Moreover, the DGEBA/MHHPA systems containing MILs displayed an additional exotherm appearing as a new peak or shoulder at temperatures between 60 and 75 °C (Figure 2a). The presence of two well-defined peaks in the DSC thermograms most likely indicates the occurrence of an additional reaction mechanism.[43] This peak was the most intense for the system with $BMIMFeCl_4$ and its intensity increased with the increasing content of the MIL (Figure S4-S6). A similar low-*T* exotherm during the curing of the epoxy-anhydride system containing $BMIMFeCl_4$ has been recently described by Freitas *et al.*, who suggested the formation of active species through the interaction of $(FeCl_4)^-$ anion and the carbonyl group of the anhydride.[35]

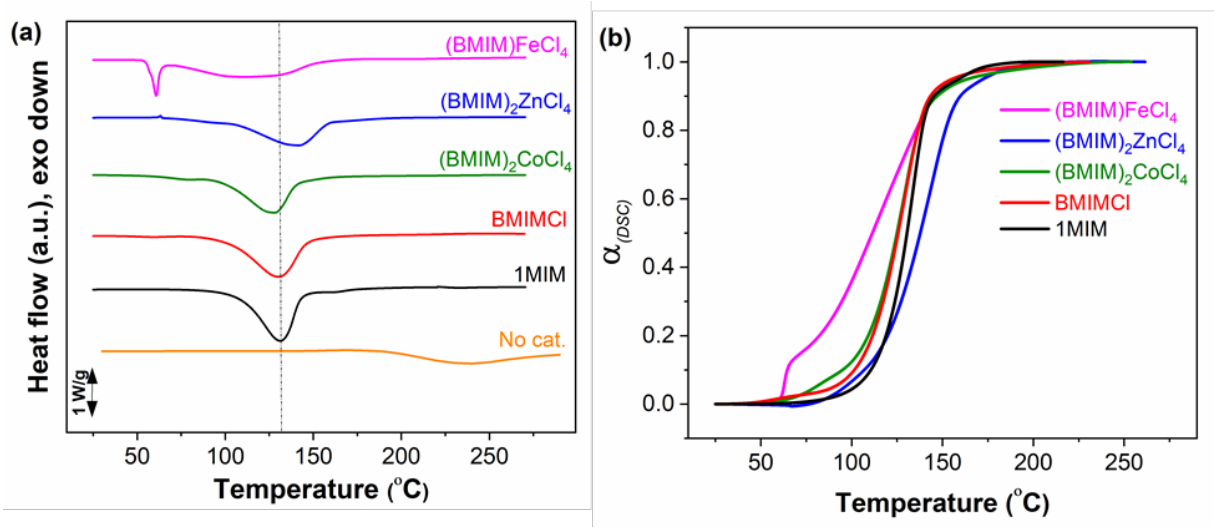

Figure 2. (a) Non-isothermal (dynamic) DSC curves and (b) conversion (α) curves during non-isothermal cross-linking of DGEBA/MHHPA with 2.70 mol% of catalyst at 5 °C/min.

The non-isothermal conversion (α_{DSC}) curves (Figure 2b) show that the addition of MILs accelerates the cross-link reaction at low temperature region (60-70 °C), where there is a sudden increase in conversion (the jump is the most noticeable for the system with $BMIMFeCl_4$), leading to a divergence from the sigmoid shape of the conversion curve, typical for the reference (imidazole-accelerated) system.

To explore more the origin of the low-T exotherm and to get a better insight on the curing mechanism of DGEBA/MHHPA/MILs systems, the non-isothermal cross-linking (heating rate of 5 °C/min) was monitored using NIR spectroscopy, which enabled us to follow the evolution of the characteristic bands of epoxy (4530 cm^{-1}), anhydride (4828 cm^{-1}), ester (5158 cm^{-1}), hydroxyl (the broad overlapping OH bands of alcohol and carboxylic acid functionalities in the region of 6800 − 7130 cm^{-1}) groups and moisture (5252 cm^{-1}, Figure S7 and Table S3).[49–51] The decreased intensity of epoxy and anhydride bands with the increasing temperature during the cross-linking proved the complete curing process for all studied systems (Figure 3). Consequently, the content of ester group was gradually increased with the increasing reaction temperature. It was noticed that the anhydride consumption was always faster in the

beginning of reaction and synchronized with a decrease in moisture content, suggesting that the MHHPA ring opening was initiated by water at the initial stage of the reaction (Figure 3). A larger deviation between epoxy and anhydride conversion curves, observed before the copolymerization is initiated, can be ascribed to a higher level of moisture in the formulation owing to the hygroscopic nature of MILs. In the case of MILs-containing systems, this decrease in moisture content was connected to an increase in the hydroxyl band, appeared at 90, 110 and 60 °C, for DGEBA/MHHPA system with $(BMIM)_2CoCl_4$, $(BMIM)_2ZnCl_4$, and $BMIMFeCl_4$, respectively (Figure 3a-c). The increased intensity of OH group bands indicated the formation of carboxylic acids due to hydrolysis of anhydride ring, followed by a sudden decrease of OH, epoxy and anhydride functional groups, proving fast progress of the subsequent esterification reaction. This reaction route was the most significant in the case of DGEBA/MHHPA system with $BMIMFeCl_4$.

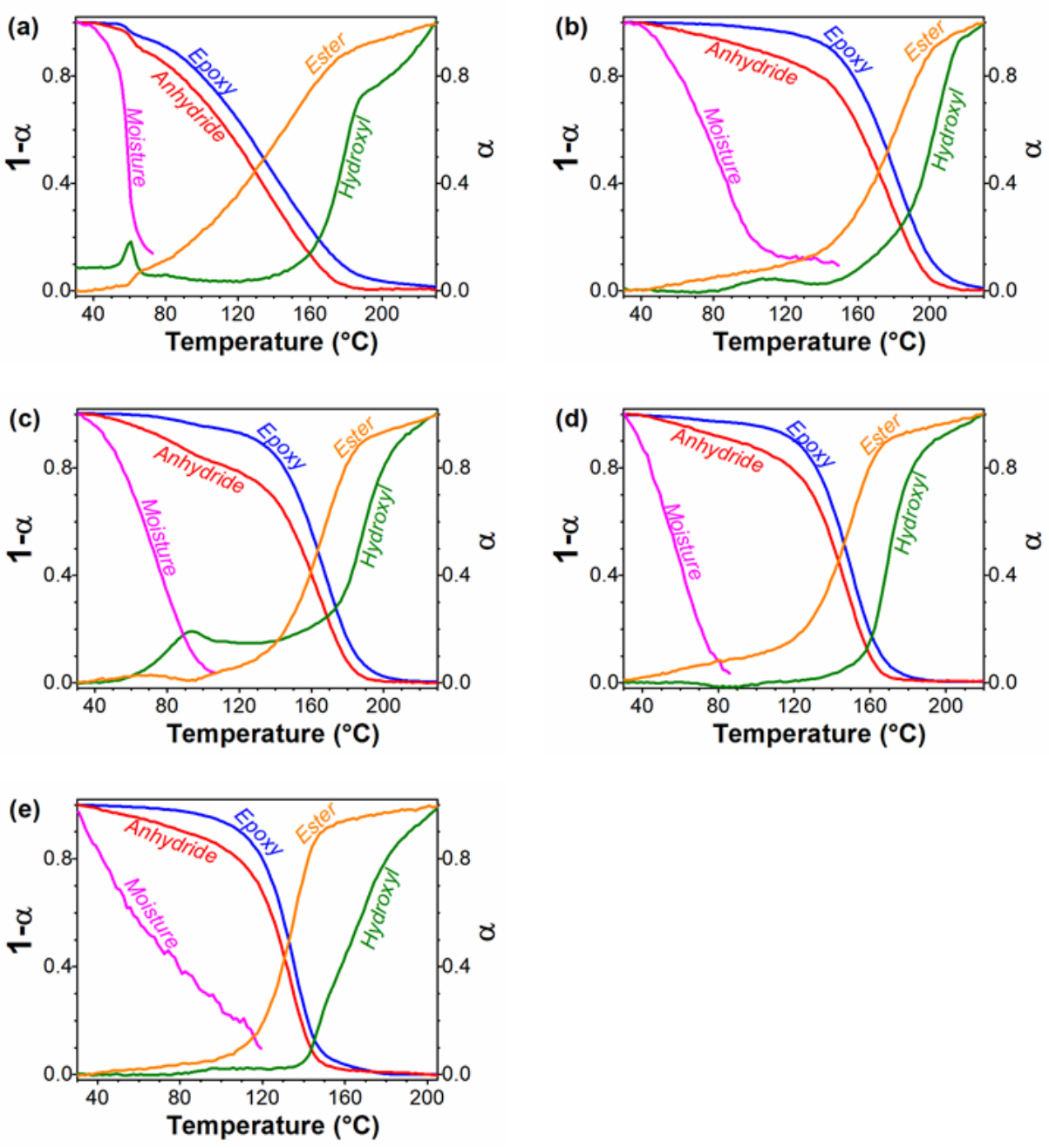

Figure 3. Development of content of function groups according to NIR spectroscopy. Non-isothermal (5 °C/min) cross-linking of DGEBA/MHHPA with different accelerating agents (2.7 mol%): (a) $BMIMFeCl_4$, (b) $(BMIM)_2ZnCl_4$, (c) $(BMIM)_2CoCl_4$, (d) BMIMCl, and (e) 1MIM. Left Y-axis for Epoxy, Anhydride and Moisture; Right Y-axis for Ester and Hydroxy.

To reach more information about the low-T process, the DGEBA/MHHPA/$BMIMFeCl_4$ formulation was followed under isothermal conditions at 60 °C (Figure S8a), showing initial

fast hydrolysis of anhydride, proved by the decrease of anhydride and moisture bands, followed by a temporary increase of the OH band (due to COOH groups formation) and a final fast consumption of carboxylic functions due to their reaction with epoxy ring and OH groups producing ester linkages, indicated by the sudden decrease of OH and epoxy bands, and the increase of ester band. Furthermore, the process is almost stopped when acidic functions are consumed (after ca 6 min at 60 °C, Figure S8a). Then, the decrease of epoxy and anhydride bands begin to be moderate and synchronous, implying a slow subsequent alternating copolymerization (Figure S8a).

At the later stage of curing (at *T* above ca 100 °C), the consumption of epoxy and anhydride groups was further accelerated until their full consumption was reached (at around 200 °C, Figure 3 and Figure S8b). The conversion of epoxy and anhydride groups occurred simultaneously, indicating an overall alternating copolymerization behavior.[52] The OH groups started to increase again at the last stage of the cross-linking reaction, probably due to the formation of sterically-hindered OH groups, which were inaccessible for further reaction due to topological limits of the formed highly cross-linked epoxide network.

Isothermal cross-linking of epoxy – anhydride with MILs

To explore more the accelerating effect induced by MILs and to determine kinetic parameters of cross-linking reactions, the isothermal DSC runs were performed with a constant catalyst loading of 2.70 mol%. Table S4 summarizes the calorimetric isothermal data showing that the application of MILs as accelerators allowed to reach a higher final monomer conversion compared to the reference (1MIM-catalyzed) system. Figure 4a-e compares the isothermal DSC conversion curves of all studied systems illustrating that the type of accelerating agent and the curing temperature have a crucial impact on the epoxy-anhydride kinetics.

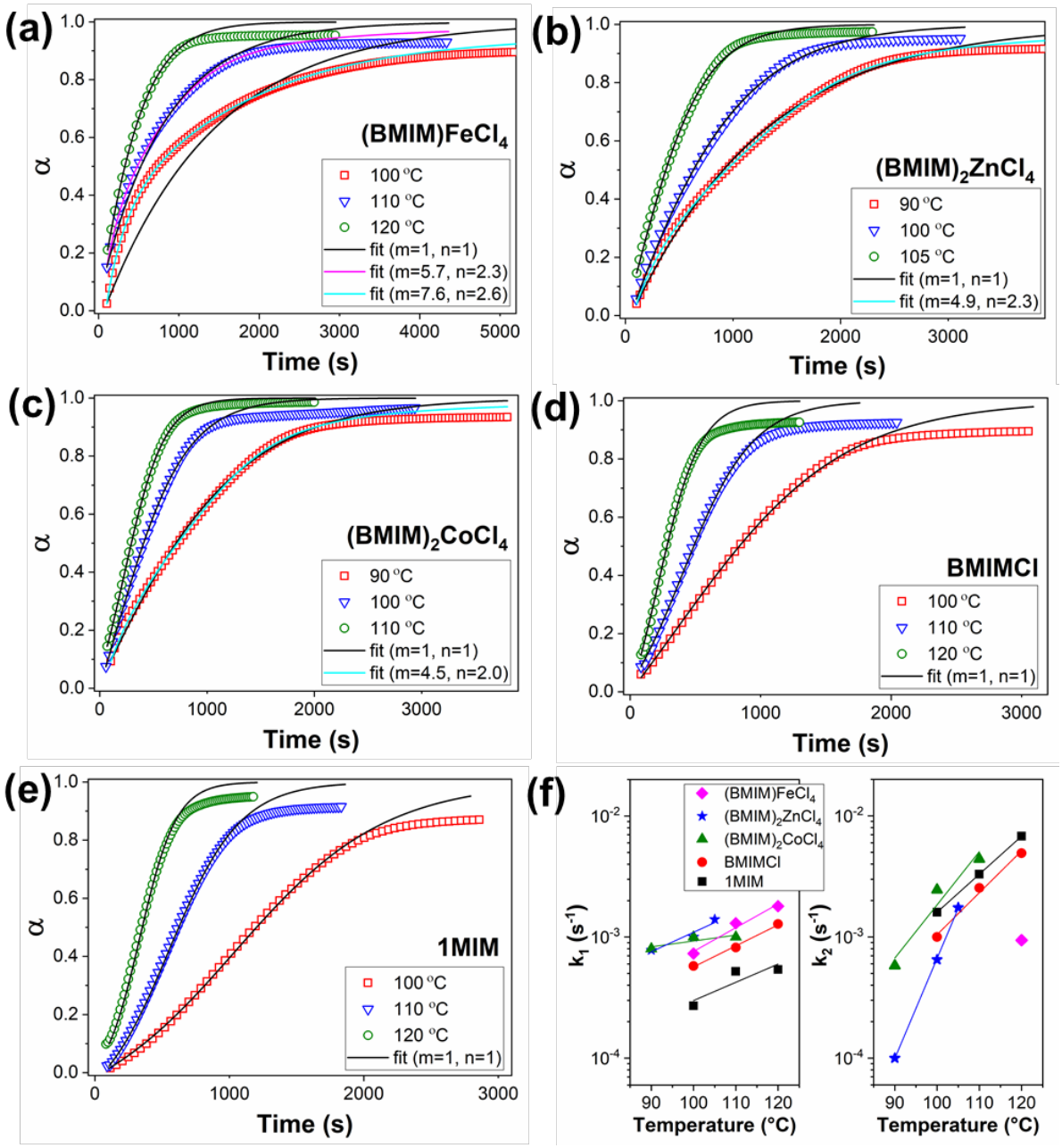

296

297 **Figure 4.** (a-e) Comparison of experimental (points) and fitted (Kamal-Sourour model fit, lines)
298 values of DSC conversion (α) during isothermal cross-linking of DGEBA/MHHPA with
299 different accelerating agents (2.70 mol%): (a) $BMIMFeCl_4$, (b) $(BMIM)_2ZnCl_4$, (c)
300 $(BMIM)_2CoCl_4$, (d) BMIMCl, and (e) 1MIM. (f) Temperature dependence of k_1 (non-catalytic)
301 and k_2 (catalytic) rate constants of Kamal-Sourour model (m=1, n=1) determined from the
302 fitting of DSC conversion (α) data during isothermal cross-linking of DGEBA/MHHPA with
303 different accelerating agents (lines are linear fits according to Arrhenius equation (9)).

To better investigate the curing kinetics, we treated the experimental results with the autocatalytic Kamal-Sourour model (see equation (7)), which adopts a model-fitting algorithm and is commonly used to describe the autocatalytic behavior of a large number of epoxy curing reactions.[47,53–55] This model proposes that the curing reaction is governed by two, non-catalytic (k_1) and catalytic (k_2) rate constants. The overall reaction order (m+n) was initially fixed to 2 based on the literature data.[53,56] The first fitting results for the reference imidazole-catalyzed system showed the partial reaction orders of m=1 and n=1 (DGEBA/MHHPA/1MIM, Figure 4e), which were kept for fitting of all systems. The model simulation correlates well with the experimental data up to conversions of about 0.80 (Figure 4), describing well the chemically controlled kinetics.[57] At the later stage of curing, the simulation data begin to diverge due to vitrification, after which the cross-linking reaction started to be a diffusion controlled.[53,58,59] This diffusion–driven reaction cannot be described by this model and new parameters must be considered to describe kinetics beyond vitrification [60], which is nevertheless out of scope of this study.

For both reference systems accelerated by either 1MIM or BMIMCl, the simulation curves fitted well the experimental values at all tested temperatures (Figure 4d,e). In contrast, the MILs-induced cross-linking (Figure 4a-c) exhibited good fitting results at higher temperatures and a certain deviation from the model at lower temperatures (100 and 110 °C for $BMIMFeCl_4$, and 90 °C for $(BMIM)_2CoCl_4$ and $(BMIM)_2ZnCl_4$). A better fit for the low-T region was obtained when all parameters (k_1, k_2, m and n) of the Kamal-Sourour model were allowed to be adjusted. Then, the fitting results for MILs-containing systems at low temperatures show an excellent agreement with the experimental conversion data (blue and magenta lines in Figure 4). However, the reaction orders (m, n) increased significantly losing their original physical meaning [10.1002/9783527828692.ch7]. In general, the reaction orders show only a low variation on the curing temperature assuming an unaltered reaction

mechanism.[61] Herein, the observed substantial increase in reaction orders, especially in the kinetic exponent *m* representing the catalytic reaction, suggests an additional cross-link mechanism proceeds at low temperatures, which is probably related to the formation of new catalytic centers induced by MILs. This observation is in good correlation with the non-isothermal DSC runs (the appearance of the second low-*T* exotherm, Figure 2) and NIR results (the fast conversion increase at the low-*T* region, Figure 3) described above.

Further insight into the kinetics of the two stages of the cross-linking is gained from the comparison of reaction rates (k_1 and k_2) listed in Table S5 and Figure 4f. For both reference DGEBA/MHHPA systems accelerated by 1MIM and BMIMCl, a typical S-shaped conversion curve was observed as a result of the two various curing steps characterized by two different rate constants (a non-catalyzed k_1 and a catalyzed k_2) with two activation barriers (E_{a1} and E_{a2}-calculated from the Arrhenius equation (9) – Figure S9-S13).[43] Usually, the non-catalytic route is dominant only at very low temperatures due to lower activation energy ($E_{a1} < E_{a2}$, Table S5). Herein, for 1MIM- and BMIMCl-accelerated curing, $k_2 > k_1$ in all tested temperature range (Figure 4f), which means that the non-catalyzed pathway (k_1) is much slower than the catalyzed route (k_2) and the cross-linking is driven by the catalytic (imidazole) pathway.[62] In contrast, the conversion curves of the MILs-accelerated systems revealed an exponential-like behavior (Figure 4). A similar behavior for the IL-cured DGEBA was attributed to a change in mechanism due to the presence of chloride anion of IL acting as an initiator / cocatalyst.[54] Therefore, the exponential kinetics observed for the MILs-induced epoxy-anhydride cross-linking can also be ascribed to a catalytic ability of MCl_4 anions, especially at low temperatures. Based on the NIR results, this MCl_4-initiated reaction pathway includes formation of carboxylic acids and their subsequent esterification (as evidenced below). The kinetic modelling shows that for MILs-containing systems at low temperatures (90 – 110 °C), the non-catalytic rate constant k_1 is always higher than k_2 (Figure 4f). This indicates that the MILs-accelerated

polyesterification pathway involving the formation of new acidic initiation centers and the subsequent rapid monomer conversion causes an increase in the k_1 rate constant. In contrast, at higher temperature the catalytic constant k_2 becomes more dominant and the cross-linking is then driven by the anionic mechanism, similar to the reference systems. The results of the kinetic study show the considerable complexity of the epoxy-anhydride cross-linking accelerated by MILs. This complicates the application of the Kamal-Sourour model, especially at low temperatures, where MILs-induced esterification is the dominant mechanism.

Overall, the activation energies (E_{a1} and E_{a2} values) for the MIL-containing systems are higher than those of the reference systems (Table S5, Figure S9-S13) and those reported in the literature for epoxy-anhydride systems (60 to 75 kJ/mol), [47,63,64] demonstrating distinct mechanism of MILs-induced epoxy-anhydride cross-linking.

Mechanism of epoxy-anhydride cross-linking induced by MILs

The above-mentioned NIR results revealed a complex DGEBA/MHHPA cross-link mechanism induced by MILs. To find out the origin of the MILs-induced epoxy-anhydride reaction, the model reactions between mono-functional epoxy resin, phenyl glycidyl ether (PGE), and MHHPA in the presence of accelerating agents (MILs, BMIMCl and 1MIM) were conducted. Supposing alternating copolymerization mechanism, the PGE/MHHPA reaction produces a linear soluble polymer, suitable for MALDI TOF mass spectrometry, allowing to determine end-groups and repeating units of the growing polymer chains. The PGE/MHHPA reactions were performed at 80 °C to explore the low-*T* curing mechanism. The MALDI-TOF mass spectra of the reaction mixtures after 15 min and the assigned structures are given in Figure 5 and Figure S14-18. First, the MALDI-TOF mass spectrum of the imidazole-catalyzed reference system (PGE/MHHPA/1MIM) was analyzed showing only one major distribution with a mass increment of 318 Da, consisting in alternating MHHPA (168 Da) and PGE (150 Da) units, and 82 Da terminal unit assigned to 1-methylimidazolium (Figure S14). This

indicates the initial step involving the nucleophilic attack of 1MIM to the oxirane ring and formation of an alkoxide.[65] In the subsequent propagation step, the alkoxide attacks an anhydride group yielding a carboxylate anion, which is able to open another oxirane ring.[66] This anionic mechanism results in the formation of a strictly alternating copolymer (Scheme S1).

The presence of MILs and BMIMCl as the accelerating agents induced the formation of five distributions of molecular ions having different end-groups but the same mass increment of 318 Da, which was composed of alternating PGE (150 Da) and MHHPA (168 Da) units (Figure 5 and Figure S15-18), confirming a strictly alternating copolymerization. The different positions of the signals in the mass spectra prove the presence of various end-groups and suggest different several initiation mechanisms. It is known that imidazolium ILs can initiate the epoxy ring opening via three main routes: carbene formation, imidazolium decomposition ('imidazole' route) and counter-ion route (anion nucleophilic attack).[36,43,67] Herein, the MALDI-TOF mass spectrometry revealed the dealkylation of butyl (the black-marked structure and signals in Figure 5) and methyl (the green-marked structure and signals in Figure 5) chains of the imidazolium ring confirming the initiation mechanism via the 'imidazole' route.[67,68] The formed dealkylated nitrogen atom causes the opening of the epoxy ring as suggested in Scheme 1a in a similar manner to the conventional imidazole catalyst (here 1MIM). Nevertheless, three dominant distributions detected in the MALDI-TOF mass spectra of all MILs-containing systems reveal the formation of structures end-capped with i) terminal Cl-opened epoxy ring (the blue-marked structure and signals in Figure 5), ii) OH (the red-marked structure and signals in Figure 5), and iii) COOH (the violet-marked structure and signals in Figure 5). The presence of Cl and OH end-groups proves the counter-ion nucleophilic initiation route. Herein, the chloride anion of MILs attacks the less hindered carbon of the oxirane ring (in similar manner as a non-metal BMIMCl[36]) forming an alkoxide anion. This anion can either directly attack another anhydride group to create a carboxylate anion[65] (Scheme 1b) or due to its willingness

to facile hydrolyzation[69] be first transformed to a hydroxy-alkoxide, which subsequently reacts with another anhydride to form a carboxylate anion (Scheme 1b). In both cases, the reaction further propagates by nucleophilic attack of carboxylate anions to another epoxy ring in an alternate manner[69] obtaining an alternating epoxy-anhydride copolymer (the blue- and red-marked structures and signals in Figure 5).

Beside this, the formation of carboxyl group end-capped alternating PGE-MHHPA copolymer chains (the violet-marked distribution and signals in Figure 5 and Figure S15-18) indicates an additional reaction pathway initiated by carboxyl groups formed during hydrolytic decomposition of anhydride rings. Considering that the formation of carboxyl groups in the low-*T* region is only visible in the case of MILs (see the NIR results above, Figure 3), it can be assumed that this initiation pathway involves formation of active species through the interaction between the MCl_4 (especially $FeCl_4$) counter-anion and anhydride ring. Freitas et *al.* suggested formation of carboxylate anions with carbonyl group linked to $FeCl_4$ counter-anion, capable to promote anionic copolymerization with oxirane ring.[35] Nevertheless, herein a different reaction mechanism is suggested based on the NIR and MALDI-TOF mass spectrometry results. Due to the Lewis acid character of the MILs [69], an anhydride-MCl_4 counter-anion complex is firstly formed (Scheme 1c). The generated complex facilitates an attack of trace amount of water (presumably originating from hygroscopic ILs), which leads to hydrolysis of the cyclic anhydride producing two carboxyl groups. The acidic proton of the carboxylic group activates the epoxy ring and caused its fast opening and formation of a hydroxyester.[65] In general, the carboxylic acid–epoxy esterification is slow and therefore only significant at high temperatures.[62] However, herein the initiation of the polyesterification pathway is highly accelerated by MILs, which causes fast conversion of the anhydride groups to the hydroxyesters at low temperatures and low degrees of conversion. The following propagation step comprises further esterification of the hydroxyesters by reaction with another anhydride group yielding

the alternating epoxy-anhydride copolymer with a terminal carboxyl group (Scheme 1c and the violet-marked distribution and signals in Figure 5 and Figure S16-18).

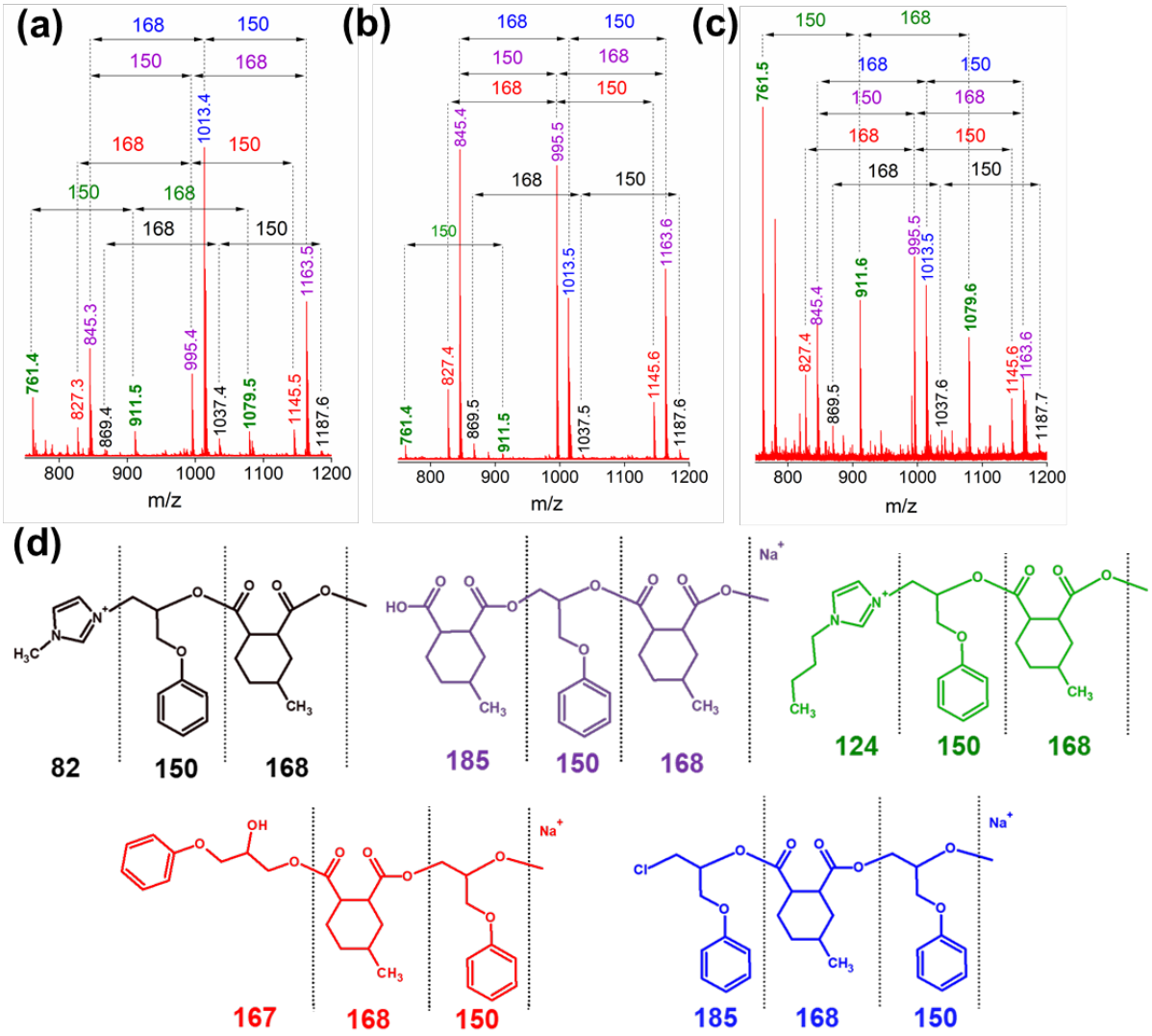

Figure 5. MALDI-TOF mass spectra (a-c) and assigned structures (d) of PGE/MHHPA reaction mixture after 15 min reaction at 80 °C accelerated by (a) $BMIMFeCl_4$, (b) $(BMIM)_2ZnCl_4$, and (c) $(BMIM)_2CoCl_4$. The whole-range MALDI TOF mass spectra are available in SI.

Altogether, the MILs-accelerated hydrolysis of anhydride ring and the subsequent polyesterification substantially affect the overall epoxy-anhydride kinetics of cross-linking (as mentioned above). The MILs demonstrated a faster initiation of the epoxy-anhydride reaction

and an overall higher reactivity when compared to the conventional non-metallic BMIMCl. This is attributed to the incorporation of the metal chloride anions into the structure of ILs, thereby enhancing its acidity.[70] Numerous studies have proved that chlorometallate ILs exhibit a more pronounced Lewis acid character than conventional ILs.[28,30,70,71] This is controlled by the electrophilicity of the metal and by the mole fraction of the metal chloride used in MIL synthesis.[29] The pronounced Lewis acid property makes the MIL effective catalysts in various reactions, thereby manifesting efficient catalysis in the epoxy-anhydride curing reaction.

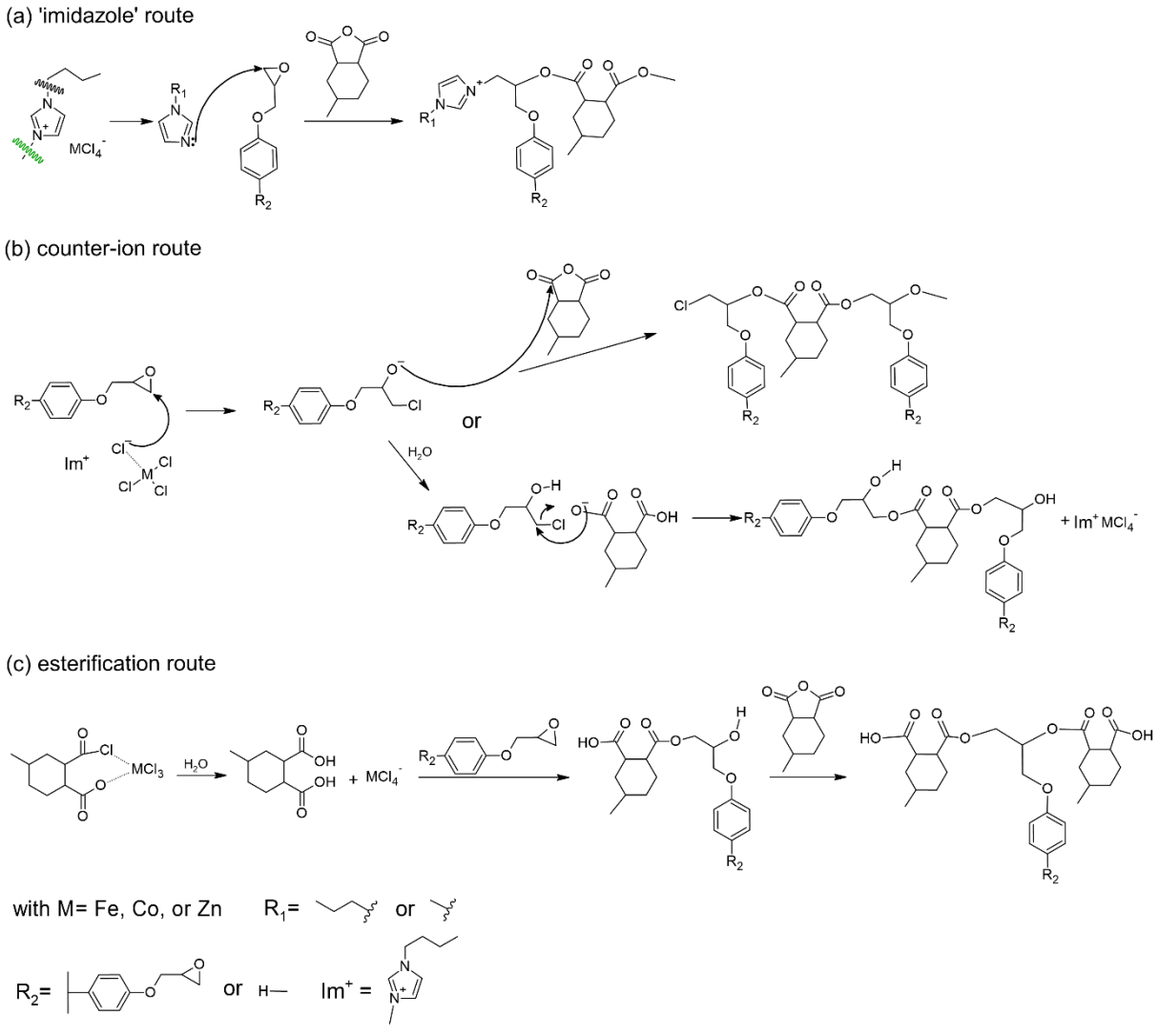

Scheme 1. Proposed mechanisms of epoxy-anhydride reaction initiated by MILs via (a) 'imidazole', (b) counter-ion, and (c) esterification route.

Thermal and mechanical properties of the obtained networks

The first sign of the overall perspective of using MILs as accelerating agents for the epoxy-anhydride cross-linking can be seen from the achievement of a high T_g of the cross-linked networks after the dynamic DSC runs (Table S2). For deeper investigation of properties of the MIL-induced networks, the amount of the accelerating agents was first optimized using the dynamic DSC runs of reactive systems with different amounts of accelerating agents aiming to reach complete cross-link reaction (maximal reaction enthalpy, ΔH) and three-dimensional network build-up (maximal T_g, Table S6).[72] It was found that the amount of 0.33, 1.0 and 1.0 mol% of $BMIMFeCl_4$, $(BMIM)_2CoCl_4$, and $(BMIM)_2ZnCl_4$, respectively, was optimal as the fabricated epoxy-anhydride networks with the highest T_g values while the content of MILs was kept at the lowest possible level. Minimal concentration of accelerating agent has to be reached to ensure that all reactive moieties can be activated[73] avoiding incomplete cross-linking (indicated by the lowered ΔH and T_g values in Table S6). On the other hand, too high contents of accelerating agents caused lowering of T_g (Table S6) due to plasticizing effect.[35] It is worth mentioning that the optimal amount in the case of $BMIMFeCl_4$ was found to be 7-fold lower compared to the non-metallic BMIMCl and more than 3-fold lower compared to the conventional 1MIM catalyst, which is advantageous from an environmental and economic point of view.

After optimization, all reactive systems were subjected to a complete curing cycle (including the post curing step at elevated temperature – see experimental part) and the thermomechanical properties of the final epoxy-anhydride networks were evaluated (Figure 6a,c and Table 2). DMTA shows a one-step change in storage modulus (G') and a single distinct relaxation $\tan\delta$ peak at 155-160 °C corresponding to the T_g, which indicates a homogeneous network structure for all samples with the exception of the DGEBA/MHHPA/BMIMCl and DGEBA/MHHPA/$(BMIM)_2ZnCl_4$ samples. In these cases,

474 the peak shoulder on the tan δ curve in a sub-glass transition region (around 100 °C) appeared,
475 showing a partly heterogeneous network structure[66], probably due to the presence of less cross-
476 link local domains.[74] However, for all MILs-containing materials, the T_g values were higher
477 than those of the reference DGEBA/MHHPA/1MIM showing formation of overall dense
478 networks. These findings are in accordance to a determined high G' values at the rubbery region
479 (Figure 6a). The calculated values of cross-link density (v_e) and average molecular mass
480 between cross-links (M_c) of the MILs-containing samples (Table 2) indicate the formation of
481 highly cross-linked networks as the result of several cross-link mechanisms during epoxy-
482 anhydride network build-up. The highest v_e achieved for the $BMIMFeCl_4$-containing material
483 correlates well with the largest extent of the low-T esterification cross-link pathway (as
484 suggested in Scheme 1c) in this sample (see the DSC and NIR results above). This suggests
485 that DGEBA/MHHPA networks cured with MILs present not only fast curing but also produce
486 epoxy networks with improved thermo-mechanical properties, which makes these compounds
487 promising agents for newly developed epoxy materials.

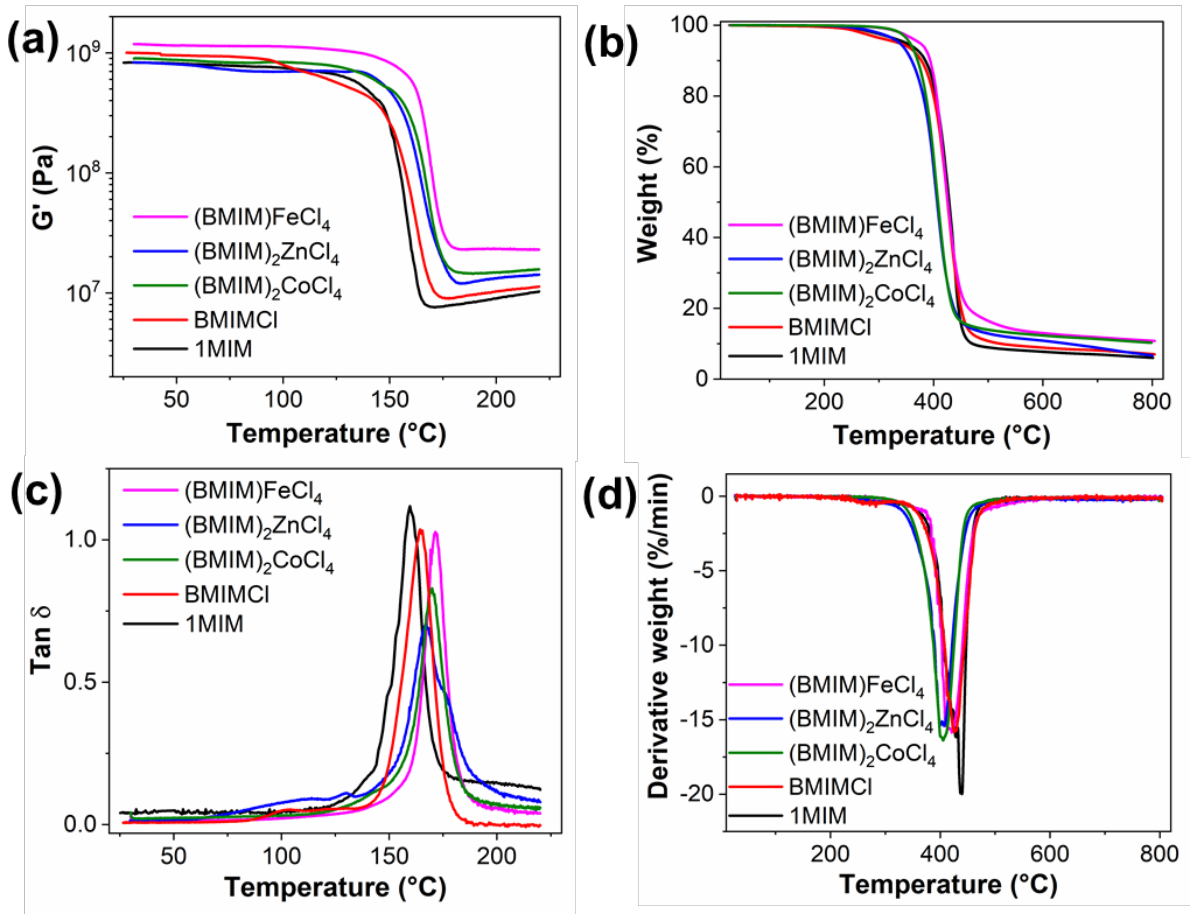

Figure 6. The DMTA (a,c) and TGA (b,d) results of the epoxy-anhydride networks fabricated using different accelerating agents: temperature dependence of (a) storage modulus (G') and (c) loss factor (tan δ), and (b) thermogravimetric and (d) derivative weight curves during TGA under N_2 atmosphere.

Table 2. Results of dynamic mechanical and thermal analysis (T_α - maximum of the tan δ peak, M_c - molecular weight between cross-links and v_e - cross-link density) and thermogravimetric analysis (T_{d5}, T_{d10}, T_{dmax} - temperatures at 5%, 10% and maximum mass loss, and char yield) of the epoxy-anhydride networks prepared using different accelerator agents.

Accelerator agent			T_α	M_c	v_e	T_{dmax}	T_{d5}	T_{d10}	Char
	mol%	wt%	(°C)	(g/mol)	(mmol/cm^3)	(°C)	(°C)	(°C)	(wt.%)
1MIM	2.7	1.3	164	490	2.4	437	349	385	7.0
BMIMCl	2.7	2.8	160	435	2.7	427	333	376	8.1
$BMIMFeCl_4$	0.2	0.4	171	207	5.6	419	374	393	11.8
$(BMIM)_2ZnCl_4$	1.0	2.8	167	343	3.4	407	337	359	8.9
$(BMIM)_2CoCl_4$	1.0	2.8	170	308	3.8	406	356	370	11.4

The influence of the added MILs on the thermal stability of the final networks was evaluated using TGA, which shows a single decomposition step for all samples (Figure 6b,d). The best thermal stability (the highest T_{d5} and T_{d10} values) and the enhanced char-forming ability were observed for the DGEBA/MHHPA samples containing $BMIMFeCl_4$ and $(BMIM)_2CoCl_4$, which can be explained by the combination of network homogeneity (see also the DMTA results in Figure 6a,c), high cross-link density (Table 2), and the presence of thermally stable metal anions.[75] In general, the epoxy networks bearing MILs displayed a higher char yields (8.9 - 11.8 wt%) than those with 1MIM and BMIMCl (7.0 - 8.1 wt%, respectively). This char residue improvement is mainly due to the formation of highly cross-linked structure and the presence of the anionic part of the IL that contains a metal center (Fe, Co, Zn). This could exert a protection of the epoxy matrix from combustion by prohibiting the transfer of volatile compounds and heat through a heat barrier effect.[76] To conclude, the addition of MILs for epoxy-anhydride cross-linking produces DGEBA/MHHPA networks with excellent thermal stability and high char yield.

CONCLUSION

In this work, we have shown that 1-butyl-3-methylimidazolium-based metal ionic liquids (MILs) containing anions such as, $(FeCl_4)^-$, $(ZnCl_4)^{2-}$, and $(CoCl_4)^{2-}$ can be used as accelerators for epoxy-anhydride cross-linking reactions, particularly epoxy-anhydride copolymerization (DGEBA-MHHPA). MILs were found to significantly accelerate the DGEBA-MHHPA cross-linking reaction, especially at low temperatures (60-80°C) due to their ability to activate a rapid hydrolytic decomposition of the anhydride ring and the subsequent formation of carboxyl groups, which further initiate polyesterification. A detailed investigation of the polymerization initiation mechanism revealed the formation of an alternating epoxy-anhydride copolymer. A complex initiation mechanism induced by of MILs was revealed taking place via several pathways, specifically, the so-called imidazole route, the counter anion, and the above-mentioned polyesterification. A detailed isothermal kinetic study was performed by adopting the autocatalytic Kamal-Sourour model, and the constant rates and activation energies of the investigated systems were adequately determined. The produced epoxy networks are highly cross-linked thermosets exhibited with a high glass transition temperature (approximately 150°C), and very good thermal resistance.

Our comprehensive investigation demonstrates that MILs are effective accelerators of epoxy – anhydride cross-linking, allowing fast curing at low temperature. Moreover, the produced thermosetting materials with a high T_g, enhanced cross-linked density and very good thermal resistivity. From this point of view, we believe that the studies disclosed herein provide valuable insight into the use of MILs as prospective accelerators for the high-tech epoxy materials.

Acknowledgement

We gratefully acknowledge financial support from the Czech Science Foundation (project no. 22-05244S).

References

(1) Longo, J. M.; Sanford, M. J.; Coates, G. W. Ring-Opening Copolymerization of Epoxides and Cyclic Anhydrides with Discrete Metal Complexes: Structure-Property Relationships. *Chem. Rev.* **2016**, *116* (24), 15167–15197. https://doi.org/10.1021/acs.chemrev.6b00553.

(2) Barabanova, A. I.; Lokshin, B. V.; Kharitonova, E. P.; Afanasyev, E. S.; Askadskii, A. A.; Philippova, O. E. Curing Cycloaliphatic Epoxy Resin with 4-Methylhexahydrophthalic Anhydride: Catalyzed vs. Uncatalyzed Reaction. *Polymer (Guildf).* **2019**, *178* (April), 121590. https://doi.org/10.1016/j.polymer.2019.121590.

(3) Barabanova, A. I.; Lokshin, B. V.; Kharitonova, E. P.; Karandi, I. V.; Afanasyev, E. S.; Askadskii, A. A.; Philippova, O. E. Cycloaliphatic Epoxy Resin Cured with Anhydride in the Absence of Catalyst. *Colloid Polym. Sci.* **2019**, *297* (3), 409–416. https://doi.org/10.1007/s00396-018-4430-8.

(4) Liu, T.; Zhang, S.; Hao, C.; Verdi, C.; Liu, W.; Liu, H.; Zhang, J. Glycerol Induced Catalyst-Free Curing of Epoxy and Vitrimer Preparation. *Macromol. Rapid Commun.* **2019**, *40* (7), 1–6. https://doi.org/10.1002/marc.201800889.

(5) Zhao, W.; An, L.; Wang, S. Recyclable High-Performance Epoxy-Anhydride Resins with DMP-30 as the Catalyst of Transesterification Reactions. *Polymers (Basel).* **2021**, *13* (2), 1–18. https://doi.org/10.3390/polym13020296.

(6) Parameswaranpillai, J.; Hameed, N.; Pionteck, J.; Woo, E. M. *Handbook of Epoxy Blends*; 2017. https://doi.org/10.1007/978-3-319-40043-3.

(7) Yang, Z.; Peng, H.; Wang, W.; Liu, T. Crystallization Behavior of Poly(ε-Caprolactone)/Layered Double Hydroxide Nanocomposites. *J. Appl. Polym. Sci.* **2010**, *116* (5), 2658–2667. https://doi.org/10.1002/app.

(8) Leguizamon, S. C.; Powers, J.; Ahn, J.; Dickens, S.; Lee, S.; Jones, B. H. Polymerization-Induced Phase Separation in Rubber-Toughened Amine-Cured Epoxy Resins: Tuning Morphology from the Nano- To Macro-Scale. *Macromolecules* **2021**, *54* (17), 7796–7807. https://doi.org/10.1021/acs.macromol.1c01208.

(9) Reuther, P.; Dünnwald, P.; Tabatabai, M.; Schuh, C.; Hartmann, L.; Ritter, H. Thermally Controlled Acceleration of Epoxy Resin Curing through Polymer-Bound Imidazole Derivatives with High Latency. *ACS Appl. Polym. Mater.* **2022**, *4* (2), 1150–1158. https://doi.org/10.1021/acsapm.1c01568.

(10) Fantoni, A.; Koch, T.; Baudis, S.; Liska, R. Synthesis and Characterization of Homogeneous Epoxy Networks: Development of a Sustainable Material Platform Using Epoxy-Alcohol Polyaddition. *ACS Appl. Polym. Mater.* **2022**. https://doi.org/10.1021/acsapm.2c01728.

(11) Ooi, S. K.; Cook, W. D.; Simon, G. P.; Such, C. H. DSC Studies of the Curing Mechanisms and Kinetics of DGEBA Using Imidazole Curing Agents. *Polymer (Guildf).* **2000**, *41* (10), 3639–3649. https://doi.org/10.1016/S0032-3861(99)00600-X.

(12) Döring, M.; Arnold, U. Polymerization of Epoxy Resins Initiated by Metal Complexes. *Polym. Int.* **2009**, *58* (9), 976–988. https://doi.org/10.1002/pi.2618.

(13) Vidil, T.; Tournilhac, F.; Musso, S.; Robisson, A.; Vidil, T.; Tournilhac, F.; Musso, S.; Robisson, A.; Leibler, L. Control of Reactions and Network Structures of Epoxy Thermosets To Cite This Version : HAL Id : Hal-02135163. **2019**.

(14) Sarazin, Y.; Carpentier, J. F. Discrete Cationic Complexes for Ring-Opening Polymerization Catalysis of Cyclic Esters and Epoxides. *Chem. Rev.* **2015**, *115* (9), 3564–3614. https://doi.org/10.1021/acs.chemrev.5b00033.

(15) Amirova, L. R.; Burilov, A. R.; Amirova, L. M.; Bauer, I.; Habicher, W. D. Kinetics and Mechanistic Investigation of Epoxy-Anhydride Compositions Cured with Quaternary Phosphonium Salts as Accelerators. *J. Polym. Sci. Part A Polym. Chem.* **2016**, *54* (8), 1088–1097. https://doi.org/10.1002/pola.27946.

(16) Dmytro Ryzhakov,[a] Gaël Printz,[b] Béatrice Jacques,[b] Samir Messaoudi,[a] Françoise Dumas, [a] Samuel Dagorne*[b] and Franck Le Bideau*. Organo-Catalyzed/Initiated Ring Opening Co-Polymerization of Cyclic Anhydrides and Epoxides: An Emerging Story. *Sci. Twent. Century* **2013**, 547–563. https://doi.org/10.4324/9781315079097-35.

(17) Livi, S.; Baudoux, J.; Gérard, J. F.; Duchet-Rumeau, J. Ionic Liquids: A Versatile Platform for the Design of a Multifunctional Epoxy Networks 2.0 Generation. *Prog. Polym. Sci.* **2022**, *132*. https://doi.org/10.1016/j.progpolymsci.2022.101581.

(18) Binks, F. C.; Cavalli, G.; Henningsen, M.; Howlin, B. J.; Hamerton, I. Examining the Kinetics of the Thermal Polymerisation Behaviour of Epoxy Resins Initiated with a Series of 1-Ethyl-3-Methylimidazolium Based Ionic Liquids. *Thermochim. Acta* **2018**, *663* (February), 19–26. https://doi.org/10.1016/j.tca.2018.02.015.

(19) Yin, Y.; Liu, M.; Wei, W.; Zheng, C.; Gao, J.; Zhang, W.; Zheng, C.; Deng, P.; Xing, Y. DGEBA/Imidazolium Ionic Liquid Systems: The Influence of Anions on the Reactivity and Properties of Epoxy Systems. *J. Adhes. Sci. Technol.* **2018**, *32* (10), 1114–1127. https://doi.org/10.1080/01694243.2017.1402402.

(20) Binks, F. C.; Cavalli, G.; Henningsen, M.; Howlin, B. J.; Hamerton, I. Examining the Nature of Network Formation during Epoxy Polymerisation Initiated with Ionic Liquids. *Polymer (Guildf).* **2018**, *150*, 318–325. https://doi.org/10.1016/j.polymer.2018.07.046.

(21) Welton, T. Ionic Liquids: A Brief History. *Biophys. Rev.* **2018**, *10* (3), 691–706. https://doi.org/10.1007/s12551-018-0419-2.

(22) Hallett, J. P.; Welton, T. Room-Temperature Ionic Liquids: Solvents for Synthesis and Catalysis. 2. *Chem. Rev.* **2011**, *111* (5), 3508–3576. https://doi.org/10.1021/cr1003248.

(23) Falireas, P. G.; Thomassin, J. M.; Debuigne, A. Imidazolium-Catalyzed Dynamic Ester Cross-Links towards Reprocessable Epoxy Vitrimers. *Eur. Polym. J.* **2021**, *147* (February), 110296. https://doi.org/10.1016/j.eurpolymj.2021.110296.

(24) Fonseca, E.; Demétrio da Silva, V.; Klitzke, J. S.; Schrekker, H. S.; Amico, S. C. Imidazolium Ionic Liquids as Fracture Toughening Agents in DGEBA-TETA Epoxy Resin. *Polym. Test.* **2020**, *87* (April). https://doi.org/10.1016/j.polymertesting.2020.106556.

(25) Zielinski, D.; Szpecht, A.; Hinc, P.; Maciejewski, H.; Smiglak, M. Mono N-Alkylated

DABCO-Based Ionic Liquids and Their Application as Latent Curing Agents for Epoxy Resins. *ACS Appl. Polym. Mater.* **2021**, *3* (11), 5481–5493. https://doi.org/10.1021/acsapm.1c00777.

(26) Hameed, N.; Eyckens, D. J.; Long, B. M.; Salim, N. V.; Capricho, J. C.; Servinis, L.; De Souza, M.; Perus, M. D.; Varley, R. J.; Henderson, L. C. Rapid Cross-Linking of Epoxy Thermosets Induced by Solvate Ionic Liquids. *ACS Appl. Polym. Mater.* **2020**, *2* (7), 2651–2657. https://doi.org/10.1021/acsapm.0c00257.

(27) Zazybin, A. G.; Rafikova, K.; Yu, V.; Zolotareva, D.; Dembitsky, V. M.; Sasaki, T. Metal-Containing Ionic Liquids: Current Paradigm and Applications. *Russ. Chem. Rev.* **2017**, *86* (12), 1254–1270. https://doi.org/10.1070/rcr4743.

(28) Liu, Y.; Wang, J. Lewis Acidity and Basicity of Mixed Chlorometallate Ionic Liquids: Investigations from Surface Analysis and Fukui Function. *Molecules* **2018**, *23* (10). https://doi.org/10.3390/molecules23102516.

(29) Estager, J.; Holbrey, J. D.; Swadźba-Kwaśny, M. Halometallate Ionic Liquids-Revisited. *Chem. Soc. Rev.* **2014**, *43* (3), 847–886. https://doi.org/10.1039/c3cs60310e.

(30) Berezianko, I. A.; Vasilenko, I. V.; Kostjuk, S. V. Acidic Imidazole-Based Ionic Liquids in the Presence of Diisopropyl Ether as Catalysts for the Synthesis of Highly Reactive Polyisobutylene: Effect of Ionic Liquid Nature, Catalyst Aging, and Sonication. *Polymer (Guildf).* **2018**, *145*, 382–390. https://doi.org/10.1016/j.polymer.2018.04.059.

(31) Dutra, G. V. S.; Teixeira, T. S.; Medeiros, G. A.; Abdelnur, P. V.; Hermes De Araújo, P. H.; Sayer, C.; Neto, B. A. D.; Machado, F. On the Role of Metal-Containing Imidazolium-Based Ionic Liquid Catalysts in the Formation of Tailored Polystyrene. *Ind. Eng. Chem. Res.* **2020**, *59* (50), 21685–21699. https://doi.org/10.1021/acs.iecr.0c04327.

(32) Rahmathullah, M. A. M.; Jeyarajasingam, A.; Merritt, B.; VanLandingham, M.; McKnight, S. H.; Palmese, G. R. Room Temperature Ionic Liquids as Thermally Latent Initiators for Polymerization of Epoxy Resins. *Macromolecules* **2009**, *42* (9), 3219–3221. https://doi.org/10.1021/ma802669k.

(33) Wang, Q.; Geng, Y.; Lu, X.; Zhang, S. First-Row Transition Metal-Containing Ionic Liquids as Highly Active Catalysts for the Glycolysis of Poly(Ethylene Terephthalate) (PET). *ACS Sustain. Chem. Eng.* **2015**, *3* (2), 340–348. https://doi.org/10.1021/sc5007522.

(34) Pitula, S.; Mudring, A. V. Synthesis, Structure, and Physico-Optical Properties of Manganate(II)-Based Ionic Liquids. *Chem. - A Eur. J.* **2010**, *16* (11), 3355–3365. https://doi.org/10.1002/chem.200802660.

(35) Freitas, G.; Henriques, R. R.; Calheiros, L. S.; Soares, B. G. Impact of Magnetic Ionic Liquids as Catalystson the Curing Process of Epoxy/Anhydride System: Mechanistic Investigation and Dynamic-Mechanical Analysis. *J. Appl. Polym. Sci.* **2022**, *139* (28), 1–12. https://doi.org/10.1002/app.52606.

(36) Rebei, M.; Mahun, A.; Walterová, Z.; Trhlíková, O.; Donato, R. K.; Beneš, H. VOC-Free Tricomponent Reaction Platform for Epoxy Network Formation Mediated by a

Recyclable Ionic Liquid. *Polym. Chem.* **2022**, *13* (37), 5380–5388. https://doi.org/10.1039/d2py01031c.

(37) Wang, F.; Xu, C.; Li, Z.; Xia, C.; Chen, J. Mechanism and Origins of Enantioselectivity for [BMIM]Cl Ionic Liquids and ZnCl2 Co-Catalyzed Coupling Reaction of CO2 with Epoxides. *J. Mol. Catal. A Chem.* **2014**, *385*, 133–140. https://doi.org/10.1016/j.molcata.2014.01.024.

(38) Kim, H. S.; Kim, J. J.; Kim, H.; Jang, H. G. Imidazolium Zinc Tetrahalide-Catalyzed Coupling Reaction of CO2 and Ethylene Oxide or Propylene Oxide. *J. Catal.* **2003**, *220* (1), 44–46. https://doi.org/10.1016/S0021-9517(03)00238-0.

(39) Palgunadi, J.; Kwon, O. S.; Lee, H.; Bae, J. Y.; Ahn, B. S.; Min, N. Y.; Kim, H. S. Ionic Liquid-Derived Zinc Tetrahalide Complexes: Structure and Application to the Coupling Reactions of Alkylene Oxides and CO2. *Catal. Today* **2004**, *98* (4), 511–514. https://doi.org/10.1016/j.cattod.2004.09.005.

(40) Hayashi, S.; Hamaguchi, H. O. Discovery of a Magnetic Ionic Liquid [Bmim]FeCl4. *Chem. Lett.* **2004**, *33* (12), 1590–1591. https://doi.org/10.1246/cl.2004.1590.

(41) Zhong, C.; Sasaki, T.; Jimbo-Kobayeshi, A.; Fujiwara, E.; Kobayashi, A.; Tada, M.; Iwasawa, Y. Syntheses, Structures, and Properties of a Series of Metal Ion-Containing Dialkylimidazolium Ionic Liquids. *Bull. Chem. Soc. Jpn.* **2007**, *80* (12), 2365–2374. https://doi.org/10.1246/bcsj.80.2365.

(42) Dinu, R.; Lafont, U.; Damiano, O.; Mija, A. High Glass Transition Materials from Sustainable Epoxy Resins with Potential Applications in the Aerospace and Space Sectors. *ACS Appl. Polym. Mater.* **2022**. https://doi.org/10.1021/acsapm.2c00183.

(43) Dzienia, A.; Tarnacka, M.; Koperwas, K.; Maksym, P.; Zięba, A.; Feder-Kubis, J.; Kamiński, K.; Paluch, M. Impact of Imidazolium-Based Ionic Liquids on the Curing Kinetics and Physicochemical Properties of Nascent Epoxy Resins. *Macromolecules* **2020**, *53* (15), 6341–6352. https://doi.org/10.1021/acs.macromol.0c00783.

(44) Sourour, S.; Kamal, M. R. Differential Scanning Calorimetry of Epoxy Cure: Isothermal Cure Kinetics. *Thermochim. Acta* **1976**, *14* (1–2), 41–59. https://doi.org/10.1016/0040-6031(76)80056-1.

(45) Beneš, H.; Dupuy, J.; Lutz, V.; Lortie, F.; Duchet-Rumeau, J.; Gérard, J. F. Synergetic Catalytic Effect of Carbon Nanotubes and Polyethersulfone on Polymerization of Glassy Epoxy-Based Systems - Isothermal Kinetic Modelling. *Thermochim. Acta* **2014**, *590*, 107–115. https://doi.org/10.1016/j.tca.2014.06.023.

(46) Perchacz, M.; Matějka, L.; Konefał, R.; Seixas, L.; Livi, S.; Baudoux, J.; Beneš, H.; Donato, R. K. Self-Catalyzed Coupling between Brønsted-Acidic Imidazolium Salts and Epoxy-Based Materials: A Theoretical/Experimental Study. *ACS Sustain. Chem. Eng.* **2019**, *7* (23), 19050–19061. https://doi.org/10.1021/acssuschemeng.9b04810.

(47) Wang, C. S.; Kwag, C. Cure Kinetics of an Epoxy-Anhydride-Imidazole Resin System by Isothermal DSC. *Polym. Polym. Compos.* **2006**, *14* (5), 445–454. https://doi.org/10.1177/096739110601400501.

(48) Foix, D.; Yu, Y.; Serra, A.; Ramis, X.; Salla, J. M. Study on the Chemical Modification of Epoxy/Anhydride Thermosets Using a Hydroxyl Terminated Hyperbranched

Polymer. *Eur. Polym. J.* **2009**, *45* (5), 1454–1466. https://doi.org/10.1016/j.eurpolymj.2009.02.003.

(49) Park, S. J.; Kwak, G. H.; Sumita, M.; Lee, J. R. Cure and Reaction Kinetics of an Anhydride-Cured Epoxy Resin Catalyzed by N-Benzylpyrazinium Salts Using near-Infrared Spectroscopy. *Polym. Eng. Sci.* **2000**, *40* (12), 2569–2576. https://doi.org/10.1002/pen.11387.

(50) September, R.; December, R. A Near-Infrared. **1995**, 2787–2796.

(51) González, M. G.; Cabanelas, J. C.; Baselga, J. Applications of FTIR on Epoxy Resins – Identification , Monitoring the Curing Process , Phase Separation and Water Uptake. **1988**, *2*.

(52) Rocks, J.; Rintoul, L.; Vohwinkel, F.; George, G. The Kinetics and Mechanism of Cure of an Amino-Glycidyl Epoxy Resin by a Co-Anhydride as Studied by FT-Raman Spectroscopy. *Polymer (Guildf).* **2004**, *45* (20), 6799–6811. https://doi.org/10.1016/j.polymer.2004.07.066.

(53) Tziamtzi, C. K.; Chrissafis, K. Optimization of a Commercial Epoxy Curing Cycle via DSC Data Kinetics Modelling and TTT Plot Construction. *Polymer (Guildf).* **2021**, *230* (August), 124091. https://doi.org/10.1016/j.polymer.2021.124091.

(54) Maksym, P.; Tarnacka, M.; Dzienia, A.; Matuszek, K.; Chrobok, A.; Kaminski, K.; Paluch, M. Enhanced Polymerization Rate and Conductivity of Ionic Liquid-Based Epoxy Resin. *Macromolecules* **2017**, *50* (8), 3262–3272. https://doi.org/10.1021/acs.macromol.6b02749.

(55) SOUROUR, M. R. K. and S. Kinetics and Thermal Characterization of Thermoset Cure. *J. Appl. Polym. Sci.* **1999**, *71* (14), 2401–2408. https://doi.org/10.1002/(sici)1097-4628(19990404)71:14<2401::aid-app12>3.0.co;2-c.

(56) Altuna, F. I.; Riccardi, C. C.; Marín Quintero, D. C.; Ruseckaite, R. A.; Stefani, P. M. Effect of an Anhydride Excess on the Curing Kinetics and Dynamic Mechanical Properties of Synthetic and Biogenic Epoxy Resins. *Int. J. Polym. Sci.* **2019**, *2019*. https://doi.org/10.1155/2019/5029153.

(57) Javdanitehran, M.; Berg, D. C.; Duemichen, E.; Ziegmann, G. An Iterative Approach for Isothermal Curing Kinetics Modelling of an Epoxy Resin System. *Thermochim. Acta* **2016**, *623*, 72–79. https://doi.org/10.1016/j.tca.2015.11.014.

(58) Mauri, A. N.; Galego, N.; Riccardi, C. C.; Williams, R. J. J. Kinetic Model for Gelation in the Diepoxide-Cyclic Anhydride Copolymerization Initiated by Tertiary Amines. *Macromolecules* **1997**, *30* (6), 1616–1620. https://doi.org/10.1021/ma9614048.

(59) Franieck, E.; Fleischmann, M.; Hölck, O.; Kutuzova, L.; Kandelbauer, A. Cure Kinetics Modeling of a High Glass Transition Temperature Epoxy Molding Compound (Emc) Based on Inline Dielectric Analysis. *Polymers (Basel).* **2021**, *13* (11). https://doi.org/10.3390/polym13111734.

(60) Li, Q.; Li, X.; Meng, Y. Curing of DGEBA Epoxy Using a Phenol-Terminated Hyperbranched Curing Agent: Cure Kinetics, Gelation, and the TTT Cure Diagram. *Thermochim. Acta* **2012**, *549*, 69–80. https://doi.org/10.1016/j.tca.2012.09.012.

(61) Ren, R.; Xiong, X.; Ma, X.; Liu, S.; Wang, J.; Chen, P.; Zeng, Y. Isothermal Curing Kinetics and Mechanism of DGEBA Epoxy Resin with Phthalide-Containing Aromatic Diamine. *Thermochim. Acta* **2016**, *623*, 15–21. https://doi.org/10.1016/j.tca.2015.11.011.

(62) Ferńandez-Francos, X.; Rybak, A.; Sekula, R.; Ramis, X.; Serra, A. Modification of Epoxy-Anhydride Thermosets Using a Hyperbranched Poly(Ester-Amide): I. Kinetic Study. *Polym. Int.* **2012**, *61* (12), 1710–1725. https://doi.org/10.1002/pi.4259.

(63) Flores, H. A.; Fasce, L. A.; Riccardi, C. C. On the Cure Kinetics Modeling of Epoxy-Anhydride Systems Used in Glass Reinforced Pipe Production. *Thermochim. Acta* **2013**, *573*, 1–9. https://doi.org/10.1016/j.tca.2013.09.004.

(64) Rohde, B. J.; Robertson, M. L.; Krishnamoorti, R. Concurrent Curing Kinetics of an Anhydride-Cured Epoxy Resin and Polydicyclopentadiene. *Polymer (Guildf).* **2015**, *69*, 204–214. https://doi.org/10.1016/j.polymer.2015.04.066.

(65) Fernàndez-Francos, X.; Ramis, X.; Serra, À. From Curing Kinetics to Network Structure: A Novel Approach to the Modeling of the Network Buildup of Epoxy-Anhydride Thermosets. *J. Polym. Sci. Part A Polym. Chem.* **2014**, *52* (1), 61–75. https://doi.org/10.1002/pola.26972.

(66) Giebler, M.; Sperling, C.; Kaiser, S.; Duretek, I.; Schlögl, S. Epoxy-Anhydride Vitrimers from Aminoglycidyl Resins with High Glass Transition Temperature and Efficient Stress Relaxation. *Polymers (Basel).* **2020**, *12* (5), 1–14. https://doi.org/10.3390/POLYM12051148.

(67) Binks, F. C.; Cavalli, G.; Henningsen, M.; Howlin, B. J.; Hamerton, I. Investigating the Mechanism through Which Ionic Liquids Initiate the Polymerisation of Epoxy Resins. *Polymer (Guildf).* **2018**, *139*, 163–176. https://doi.org/10.1016/j.polymer.2018.01.087.

(68) Carvalho, A. P. A.; Santos, D. F.; Soares, B. G. Epoxy/Imidazolium-Based Ionic Liquid Systems: The Effect of the Hardener on the Curing Behavior, Thermal Stability, and Microwave Absorbing Properties. *J. Appl. Polym. Sci.* **2020**, *137* (5). https://doi.org/10.1002/app.48326.

(69) de la Cruz-Martínez, F.; Buchaca, M. M. de S.; Campo-Balguerías, A. Del; Fernández-Baeza, J.; Sánchez-Barba, L. F.; Garcés, A.; Alonso-Moreno, C.; Castro-Osma, J. A.; Lara-Sánchez, A. Ring-Opening Copolymerization of Cyclohexene Oxide and Cyclic Anhydrides Catalyzed by Bimetallic Scorpionate Zinc Catalysts. *Polymers (Basel).* **2021**, *13* (10). https://doi.org/10.3390/polym13101651.

(70) Wu, W.; Lu, Y.; Ding, H.; Peng, C.; Liu, H. The Acidity/Basicity of Metal-Containing Ionic Liquids: Insights from Surface Analysis and the Fukui Function. *Phys. Chem. Chem. Phys.* **2015**, *17* (2), 1339–1346. https://doi.org/10.1039/c4cp04603j.

(71) Taylor, A. W.; Men, S.; Clarke, C. J.; Licence, P. Acidity and Basicity of Halometallate-Based Ionic Liquids from X-Ray Photoelectron Spectroscopy. *RSC Adv.* **2013**, *3* (24), 9436–9445. https://doi.org/10.1039/c3ra40260f.

(72) Fache, M.; Auvergne, R.; Boutevin, B.; Caillol, S. New Vanillin-Derived Diepoxy Monomers for the Synthesis of Biobased Thermosets. *Eur. Polym. J.* **2015**, *67*, 527–538. https://doi.org/10.1016/j.eurpolymj.2014.10.011.

(73) Couture, G.; Granado, L.; Fanget, F.; Boutevin, B.; Caillol, S. Limonene-Based Epoxy: Anhydride Thermoset Reaction Study. *Molecules* **2018**, *23* (11). https://doi.org/10.3390/molecules23112739.

(74) Varley, R. J.; Dao, B.; Nguyen, T.; Lee, S.; Nishino, T. Effect of Aromatic Substitution on the Cure Reaction and Network Properties of Anhydride Cured Triphenyl Ether Tetraglycidyl Epoxy Resins. *Polym. Adv. Technol.* **2019**, *30* (6), 1525–1537. https://doi.org/10.1002/pat.4584.

(75) Zheng, C.; Liu, M.; Yin, Y.; Zhang, Y.; Wei, W.; Deng, P.; Zheng, C. Kinetics and Thermal Properties of Epoxy Resins Containing the Ionic Liquid [C6mim]FeCl4. *RSC Adv.* **2016**, *6* (14), 11407–11411. https://doi.org/10.1039/c5ra26150c.

(76) Zhi, M.; Liu, Q.; Chen, H.; Chen, X.; Feng, S.; He, Y. Thermal Stability and Flame Retardancy Properties of Epoxy Resin Modified with Functionalized Graphene Oxide Containing Phosphorus and Silicon Elements. *ACS Omega* **2019**, *4* (6), 10975–10984. https://doi.org/10.1021/acsomega.9b00852.